BMC Plant Biology

RESEARCH

Open Access

Comparative physiological and co-expression network analysis reveals potential hub genes and adaptive mechanisms responsive to NaCl stress in peanut (*Arachis hypogaea* L.)

Nan Zhang[1], Baiyi Bai[2], Shiyu Zuo[2], He Zhang[1], Jingyao Ren[1], Zhenghao Lv[1], Dongying Zhou[1] and Haiqiu Yu[1,2*]

Abstract

Background Salt stress has become a major threat to peanut yield and quality, and salt stress is particularly detrimental to seedling growth. Combined analysis of the physiology and transcriptomics of salt-tolerant variety (NH5) and salt-sensitive variety (FH23) under 200 mM NaCl stress was conducted to identify the key factors influencing the differences in salt tolerance and to investigate the potential regulatory mechanisms and hub genes associated with salt tolerance in peanuts.

Results Malondialdehyde (MDA) content and electrolyte leakage rate were significantly increased under prolonged NaCl stress, with the increase in FH23 being even more pronounced. NH5 maintained intracellular osmotic homeostasis by accumulating free proline and soluble protein content. In addition, NH5 exhibited higher antioxidant enzyme activity. The net photosynthetic rate (Pn) of NH5 and FH23 decreased by 64.24% and 94.49% after 96 h of stress. The intercellular CO_2 concentration (Ci) of NH5 significantly decreased by 7.82%, while that of FH23 increased by 42.74%. This suggests that non-stomatal limiting factors were the primary cause of the decline in photosynthesis observed in FH23. Transcriptome analysis revealed the presence of 12,612 differentially expressed genes (DEGs) in response to salt stress, with FH23 exhibiting a greater number than NH5. The number of upregulated genes was significantly higher than that of downregulated genes at 24 h of salt stress, whereas the number of downregulated genes exceeded that of upregulated genes at 48 h. Subsequently, Weighted Gene Co-expression Network Analysis (WGCNA) was performed in conjunction with physiological data. Twenty-four hub genes of salt response were identified, which encoded delta-1-pyrroline-5-carboxylate synthase, aldehyde dehydrogenase, SNF1-related protein kinase, magnesium transporter, temperature-induced lipocalin-1, and ERF transcription factors.

Conclusion A regulatory network for potential salt tolerance in peanuts has been constructed. The findings revealed distinct mechanisms of response to salt tolerance and identified candidate genes for further investigation.

Keywords Peanut, NaCl stress, Transcriptome sequencing, Weighted gene co-expression analysis, Differentially expressed genes

*Correspondence:
Haiqiu Yu
yuhaiqiu@syau.edu.cn
Full list of author information is available at the end of the article

Introduction

Approximately 33% of irrigated farmland and 1 billion hm^2 of cropland are affected by soil salinity worldwide [1]. The area and extent of cropland impacted by salinization are increasing annually due to climate change and the over-cultivation of farmland [2]. Soil salinization is one of the most pressing environmental issues globally, severely restricting agricultural production and food security. However, much of the mildly or moderately salinized land is still holding potential for cultivation [3]. Peanut (*Arachis hypogaea* L.) is a vital oilseed crop, rich in protein, lipids, and vitamins, and serves as a high-quality source of plant protein [4]. Peanut exhibit a high tolerance to salinity and infertility and is planted in marginal soils frequently such as saline soils to reduce the pressure of competition for land between food crop and oilseed. Peanut growth and development can be significantly hindered by abiotic stresses, particularly soil salinity [5]. Salinity has been recognized as a critical environmental factor that can adversely affect peanut yield and quality.

Salt stress affects crops in two principal ways [6]. First, a reduction in soil water potential leads to a decreased supply of water for crop uptake which in turn hinders crop growth. Second, salt stress results in a significant accumulation of ions within the crop, disrupting the ionic balance, inducing osmotic stress, and inhibiting the activity of cellular enzymes, thereby impeding crop growth and development [7, 8]. Additionally, salt stress damages nucleic acids, cellular proteins, and membrane systems, compromising membrane stability and integrity [9, 10]. It also causes a notable increase in electrolyte leakage from plant leaves [5]. The positive correlation between the rate of electrolyte leakage and the extent of membrane damage serves as a valuable tool for elucidating the underlying physiological mechanisms of plant stress responses [11]. Malondialdehyde (MDA) is one of the products of membrane lipid peroxidation. Thus, the degree of damage to membranes can be indicated through the measurement of the MDA content [12].

Proline is an essential osmoregulatory compound that is widely found in plants. The stability of osmotic pressure within and outside the cell membrane is maintained by increasing proline levels, which enhances the water-holding capacity of the cells and prevents the rupture of the cell membrane [13]. Plants are abundant in various soluble sugars, including glucose, fructose, and sucrose, among others. These sugars play a crucial role in regulating plant stress responses. In the face of adversity, plants elevate their soluble sugar content to maintain cellular osmotic balance and mitigate damage to the organism [14]. Research has demonstrated that soluble sugars are vital for maintaining protein stability [15]. Soluble proteins in plants are hydrophilic and can bind to water molecules, thereby improving the water retention capacity of plant cells during stressful conditions [16]. Additionally, soluble proteins encompass a wide array of enzymes that are involved in plant physiological responses. By producing substantial amounts of soluble proteins, plants can sustain normal physiological functions even under adverse conditions [17]. Photosynthesis is highly sensitive to salt stress, with leaves serving as the primary organ for this process in plants [18]. The most apparent manifestation of salt stress damage occurs in the leaves, where older leaves display greater vulnerability compared to younger ones. The initial signs of damage include wilting, followed by darker necrosis, and ultimately, leaf death and abscission [19]. Research has demonstrated that under salt stress, key parameters related to plant photosynthesis, such as SPAD values, net photosynthetic rate (Pn), stomatal conductance (Gs), and intercellular CO_2 concentration (Ci), are significantly reduced [20].

The genetic enhancement of salt tolerance represents is an effective strategy for mitigating salt stress [21]. Salt tolerance in plants is a polygenic trait regulated by multiple QTL [22, 23]. Transcriptomics can be utilized to assess the expression of various genes in plants, thereby elucidating diverse biological phenomena and uncovering the gene regulatory mechanisms that govern the differential expression of genes [24, 25]. Weighted Gene Co-expression Network Analysis (WGCNA) is a systems biology approach that characterizes correlation patterns of between genes in microarray samples. WGCNA identifies clustered modules of highly correlated genes, links these modules to one another and to external sample features, and can be employed to detect associations between extensive genomes and physiological traits [14]. The peanut plant undergoes a series of physiological changes, accompanied by the differential expression of numerous genes, to endure NaCl stress.

In this study, we conducted WGCNA on physiological traits and transcriptomic data from the salt-tolerant peanut variety Nonghua5 (NH5) and the salt-sensitive peanut variety Fuhua23 (FH23). Our goal was to identify the key factors influencing the differences in salt tolerance and to elucidate the potential regulatory mechanisms underlying peanut salt tolerance. The results provide a theoretical foundation for genetic breeding and the molecular mechanism analysis of salt tolerance in peanuts.

Results

Physiological differences under NaCl stress

A distinct morphological difference was observed between salt-sensitive and salt-tolerant peanut genotypes subjected to NaCl stress. Continuous observation of the

same peanut plant clearly illustrates this notable difference [26] (Fig. S1). The electrolyte leakage rate, MDA content, free proline content, soluble protein content, and antioxidant enzyme activity were measured at different time points to more precisely elucidate the response patterns of different salt-tolerant varieties under NaCl stress (Fig. 1). The electrolyte leakage rate initially exhibited a gradual increase with the duration of stress followed by a sharp rise. The conductivity of NH5 and FH23 at 24 h increased by 5.13 times and 5.90 times compared to the baseline at 0 h, reaching 18.93 times and 22.41 times at 48 h of stress (Fig. 1A). Prolonged stress resulted in a consistent increase in MDA content, with FH23 showing a significantly greater increase than NH5. The increase in the two varieties was relatively stable during the initial stages of stress (6 h and 12 h), with no significant difference compared to the measurements taken at 0 h. The MDA content exhibited a significant upward trend as the duration of stress increased, with the increase in FH23 being even more pronounced. This led to a substantial disruption of membrane permeability (Fig. 1B).

The free proline content in the leaves of both peanut varieties exhibited an upward trend with the extension of NaCl stress duration, although the magnitude of the increases varied. The free proline content in NH5 showed a significant upward trend. In contrast, FH23 displayed a notable increase followed by a marked decline. The peak value was reached at 72 h, which was 601.75% higher than that at 0 h. This variety exhibited a significant increase followed by a substantial decrease (Fig. 1C). The soluble protein content demonstrated a significant elevation during the early stage of NaCl stress (6 h), with a more pronounced surge observed in NH5. Both varieties exhibited an initial increase, which was subsequently followed by a decrease as the duration of stress increased. NH5 demonstrated the ability to maintain stable osmotic pressure by accumulating osmoregulatory substances (Fig. 1D).

The activities of SOD, POD, APX and CAT in FH23 leaves were found to be significantly lower than those observed in NH5 leaves when subjected to continuous NaCl stress. During the initial phase of the stress response, SOD activity in NH5 leaves was significantly increased, peaking at 6 h (400.18 U g^{-1} FW), which was 1.58 times higher than 0 h. As the duration of stress prolonged, SOD activity showed a slight decrease compared to the 6 h but an increase relative to the 0 h. Notably, SOD activity in FH23 remained stable (Fig. 1E). The POD activity in NH5 was maintained between 1282.49 U g^{-1} FW and 1972.49 U g^{-1} FW, while the POD activity in FH23 remained at a lower level, fluctuating between 993.93 U g^{-1} FW and 1323.17 U g^{-1} FW (Fig. 1F). Additionally, APX and CAT activity in NH5 showed a significant increase followed by a slight decline in response to continuous NaCl stress, with levels significantly higher than those observed in FH23. In contrast, FH23 exhibited a relatively gradual change, characterized by a slight initial increase that was relatively minor in amplitude (Fig. 1G-H).

Photosynthetic characteristics and chlorophyll fluorescence parameters under NaCl stress

Pn, Gs, Tr, and Ci of NH5 and FH23 decreased significantly after 6 h of NaCl stress, with further reductions observed as the duration of NaCl stress increased. Pn, Gs, and Tr exhibited a continuous and significant decline, although the magnitude of these decreases varied. Specifically, Pn decreased by 64.24% and 94.49% in NH5

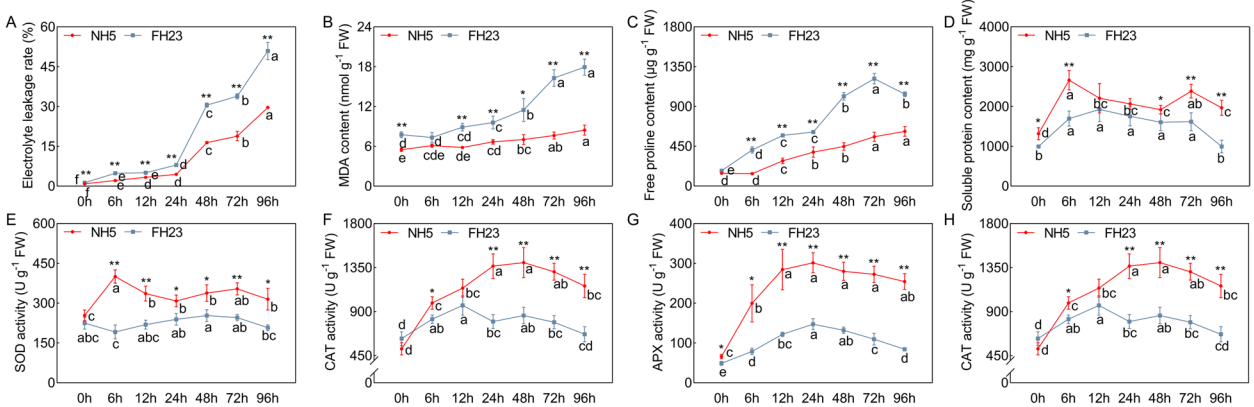

Fig. 1 Physiological differences between NH5 and FH23 under NaCl stress. **A** Electrolyte leakage rate. **B** MDA content. **C** Free proline content. **D** Soluble protein content. **E** SOD activity. **F** CAT activity. **G** APX activity. **H** CAT activity. Different letters indicate significant differences between various points for each cultivar at the $p < 0.05$ level. * and ** indicated significant differences between various cultivars for each point at the 0.05 and 0.01 levels, respectively

and FH23, Gs decreased by 71.62% and 94.91%, and Tr decreased by 72.53% and 92.80%, after 96 h of stress. As the duration of stress extended Ci initially decreased before increasing with NH5 showing relatively stable changes, while FH23 exhibited more pronounced fluctuations. Notably, Ci in FH23 began to rise after 48 h, reaching significantly higher levels at 72 h, with increases of 24.43% and 42.74% at 72 h and 96 h, respectively. In summary, the photosynthetic performance of FH23 was severely compromised compared to NH5. Initially, the reduction in photosynthetic rate was attributed to stomatal limitations, but as stress duration increased, non-stomatal limitations became the primary restricting factor (Fig. 2A-D).

To further investigate the effects of NaCl stress on photosynthesis in peanut seedlings, we measured the chlorophyll fluorescence parameters. The patterns of these parameters were similar between the NH5 and FH23 at different stress durations (Fig. 2E-I). The Fv/Fm decreased significantly after 72 h and 96 h of stress, with reductions of 2.8% and 4% in NH5, and decreases of 6.07% and 17.86% in FH23. There were significant differences between the varieties. The ΦPSII, qP, and ETR of peanut were greatly affected by NaCl stress, with both varieties exhibiting a decrease at 6 h and a slight recovery at 24 h, however, the overall trend was downward, with a more pronounced decrease observed in FH23. Compared to the measurements taken at 0 h, after 96 h of stress treatment, ΦPSII decreased by 49.57% and 82.93% for NH5 and FH23, respectively. Additionally, NPQ decreased by 33.04% and 58.33%, qP decreased by 39.62% and 65.31%, and ETR decreased by 49.57% and 82.93%. Notably, the NPQ of NH5 was significantly higher than that of FH23, indicating that NH5 was more effective at dissipating excess light energy as heat, thereby providing better protection for its photosynthetic organs. The Rfd decreased with the duration of NaCl stress, with a more substantial decline observed in FH23, suggesting that its growth vigor was more severely inhibited.

Correlation analysis of physiological indicators under NaCl

In this study, correlation analyses were conducted to examine the relationships among MDA content, electrolyte leakage rate, free proline content, antioxidant enzyme activity, photosynthetic characteristics, and chlorophyll fluorescence parameters in peanuts subjected to NaCl treatment (Fig. 3). The Pearson's correlation coefficient revealed a significant negative correlation between MDA content, electrolyte leakage rate, free proline content, and chlorophyll fluorescence parameters in peanut leaves and qP, with correlation coefficients reaching of 0.91, 0.87, and 0.92, respectively. Furthermore, a significant positive correlation was observed between these variables and Ci. It indicated that there was an overlap of information among the indicators.

Transcriptome analysis under NaCl

The molecular regulatory mechanisms underlying the response of peanut seedlings to NaCl stress were systematically elucidated at the transcriptomic level through RNA sequencing (RNA-Seq) of the leaves from NH5 (ST) and FH23 (SS) peanut seedlings at 0 h, 24 h, and 48 h, respectively. After filtering out low-quality reads from the 18 samples, a total of 125.79 Gb of clean data

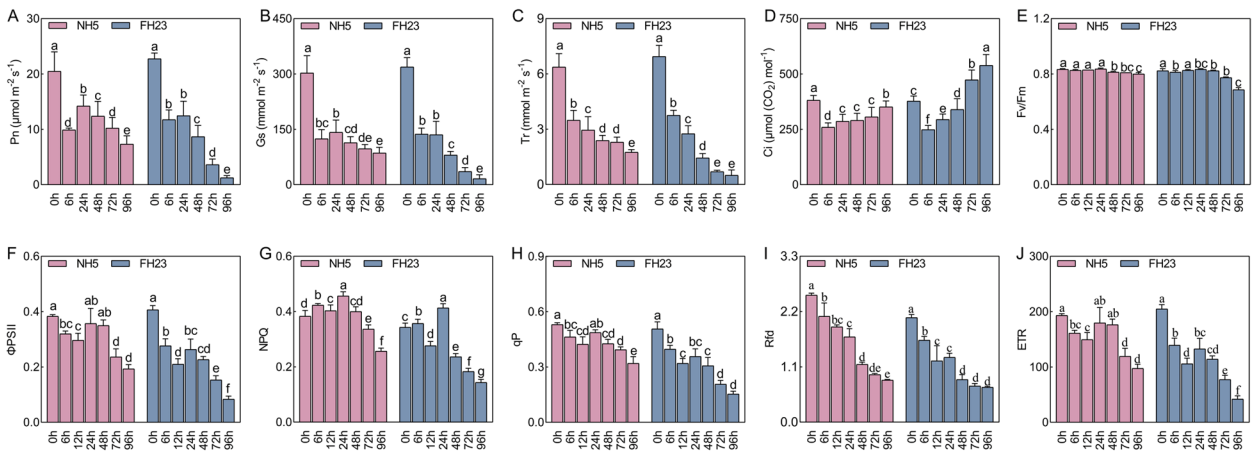

Fig. 2 Photosynthetic characteristics and chlorophyll fluorescence parameters of NH5 and FH23 under NaCl stress. **A** net photosynthetic rate (Pn). **B** stomatal conductance (Gs). **C** transpiration rate (Tr). **D** intercellular CO_2 concentration (Ci). **E** Maximum photosystem II (PSII) light quantum efficiency (Fv/Fm). **F** Actual photochemical efficiency (ΦPSII). **G** Non-photochemical quenching coefficient (NPQ). **H** Photochemical quenching coefficient (qP). **I** Fluorescence decay rate (Rfd). **J** Electron transfer rate (ETR). Different letters indicate significant differences between various points for each cultivar at the $p < 0.05$ level

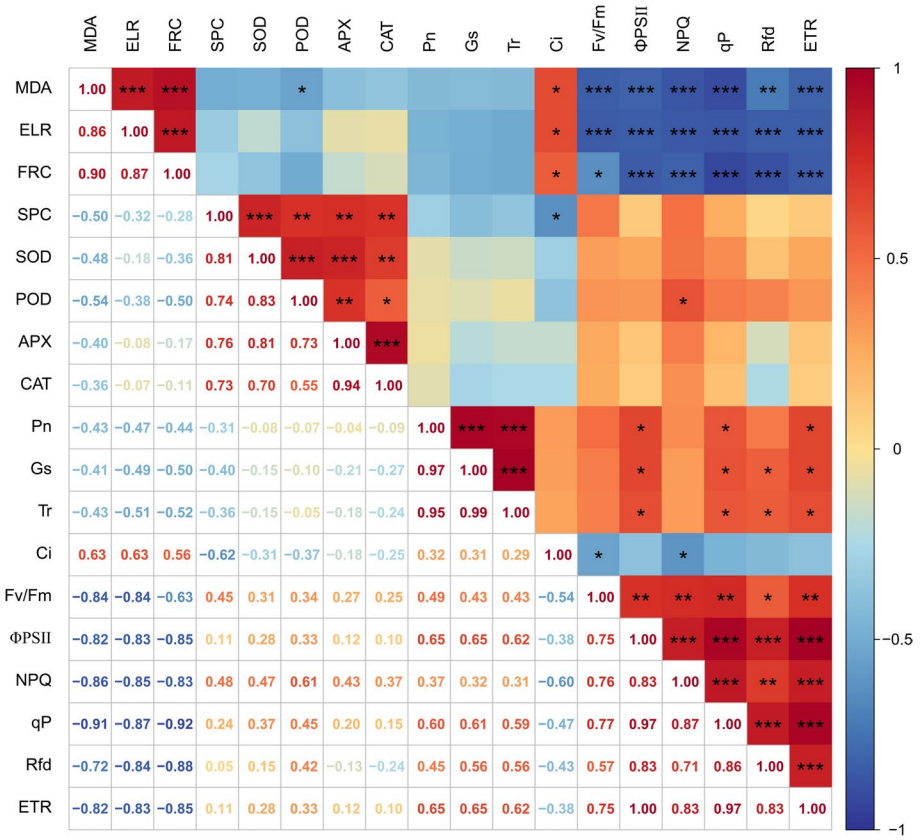

Fig. 3 Correlation matrix of physiological indices in peanut leaves. *, ** and *** indicates the correlation at the 0.05, 0.01, and 0.001 probability levels, respectively. MDA, MDA content; ELR, electrolyte leakage rate; FPC, free proline content; SPC, soluble protein content. SOD, SOD activity; CAT, CAT activity; APX, APX activity; CAT, CAT activity. Pn, net photosynthetic rate; Gs, stomatal conductance; Tr, transpiration rate; Ci, intercellular CO_2 concentration; Fv/Fm, maximum photosystem II (PSII) light quantum efficiency; ΦPSII, actual photochemical efficiency; NPQ, non-photochemical quenching coefficient; qP, photochemical quenching coefficient; Rfd, fluorescence decay rate; ETR, electron transfer rate

were obtained, with Q20 and Q30 values ranging from 92.37% to 97.7% and 92.52% to 93.32%, respectively. The comparative efficiencies were high, ranging from 95.35% to 97.7%, indicating that the transcriptome sequencing results were of good quality and suitable for subsequent analysis (Table S2). A strong correlation was observed among samples from the same replicates, while a weaker correlation was noted between different treatments. Principal component analysis revealed a similar clustering pattern (Fig. 4A-B). Differentially expressed genes (DEGs) were analyzed, resulting in a total of 12,612 DEGs. Specifically, 7,551 DEGs and 5,312 DEGs were identified in the comparisons of SS-0 h vs SS-24 h and ST-0 h vs ST-24 h, respectively. Additionally, 9,014 DEGs and 6,528 DEGs were identified in the comparisons of SS-0 h vs SS-48 h and ST-0 h vs ST-48 h, respectively. 642 DEGs were downregulated, and 882 DEGs were upregulated exclusively in SS, while 143 DEGs were specifically downregulated and 226 DEGs were upregulated in ST after 24 h of stress. The number of upregulated genes was significantly greater than that of downregulated genes. In contrast, there were 1,042 specific downregulations and 960 upregulations in SS, while ST exhibited 562 specific downregulations and 436 upregulations. After 48 h of stress, the number of downregulated genes was significantly higher than that of upregulated genes (Fig. 4C-E). qRT-PCR was conducted on 9 randomly selected DEGs to validate the results of the RNA-Seq analysis. The expression trends observed in the qRT-PCR were consistent with those of the RNA-Seq data, thereby confirming the accuracy of the RNA-Seq results (Fig. S2). RNA-Seq data have been deposited in the NCBI Sequence Read Archive (SRA) under accession number PRJNA1041034.

Construction of the co-expression network under NaCl

Based on the transcriptional databases of NH5 and FH23 under NaCl stress, the WGCNA network was constructed to gain a comprehensive understanding of the gene regulatory networks closely associated with salt tolerance in peanuts (Fig. S3). When the power parameter

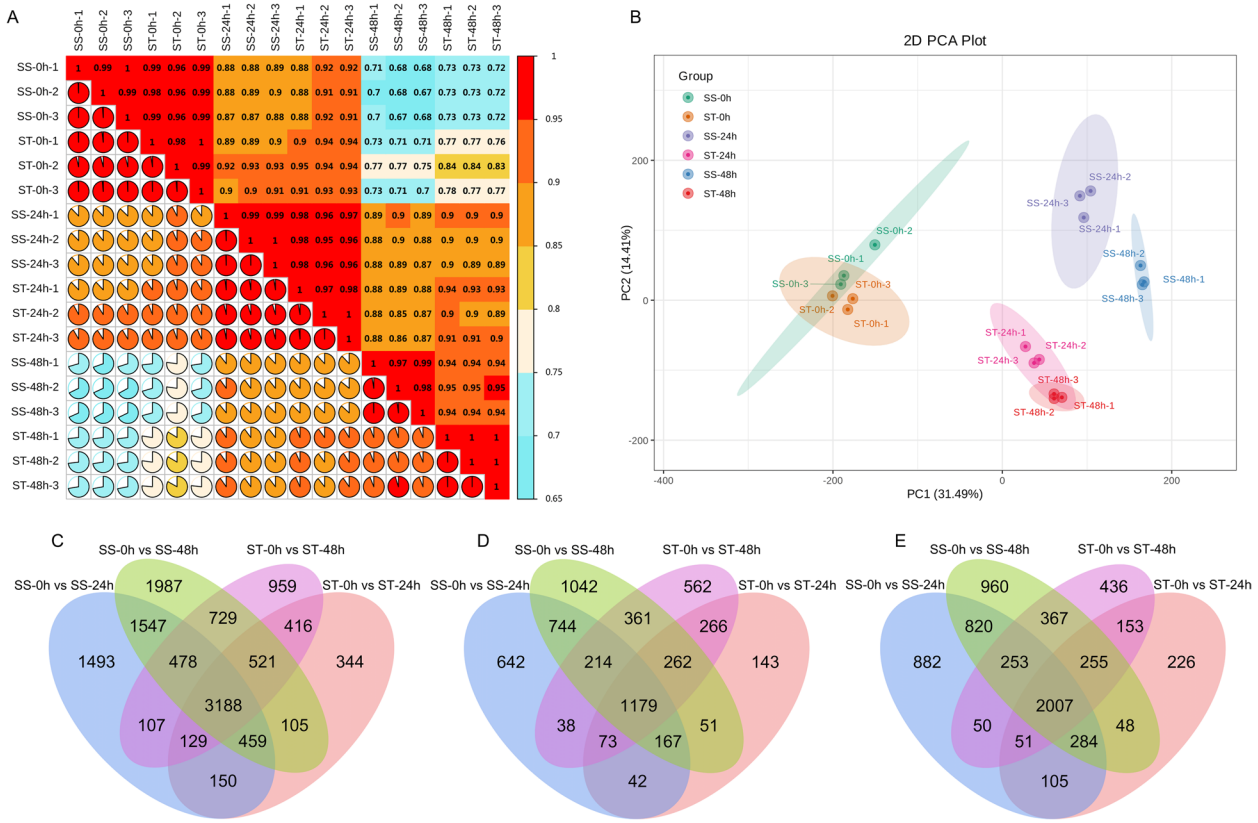

Fig. 4 Transcriptome data analysis. **A** Correlation analysis. **B** Principal component analysis. **C**-**E** Venn diagram of DEGs in NH5 and FH23 of 0 h, 24 h and 48 h. **C** All DEGs. **D** Downregulated DEGs. **E** Upregulated DEGs. ST, NH5; SS, FH23

was set to 18, the correlation coefficient (R^2) approached the plateau phase, while the mean value of the proximity function neared 0. Consequently, the power for this study was determined to be 18. Utilizing the dynamic shear method, the minimum merging height for the modules was established at 0.25, and the minimum number of genes per module was set at 30. The genes were subsequently clustered into seven distinct modules based on hierarchical clustering, with each module represented by a different color. The turquoise module contained the highest number of genes (3,968), followed by the blue module (2,271 genes), while the grey module had the fewest genes (76).

Correlation analysis between physiological traits and modules

To comprehensively explore the correlation between physiological traits and gene expression, we analyzed 18 physiological traits related to photosynthesis, membrane permeability, and antioxidant regulation using WGCNA with transcriptional data. As illustrated in Fig. 5, the turquoise, blue, and brown modules were significantly correlated with 14, 12, and 12 traits, respectively. The blue and brown modules exhibited highly significant positive correlations with MDA content, electrolyte leakage rate, osmoregulatory substance content, Gs, Tr, and Ci. Notably, the brown module displayed the highest correlation coefficients with free proline content (0.96) and electrolyte leakage rate (0.93). The turquoise module demonstrated a significant positive correlation with fluorescence parameters, particularly with the largest correlation coefficient observed for the Rfd at 0.91. Additionally, antioxidant enzyme activity showed significant positive correlations with the green and yellow modules. A higher correlation between a physiological trait and a module suggests that the module may serve as a core regulator of the physiological trait, prompting further analyses of the 5 modules: blue, brown, green, yellow, and turquoise.

Gene expression patterns of highly relevant modules and identification of key modules

The expression patterns of the 5 core modules were analyzed (Fig. S4). Genes in the same module had highly similar expression patterns. Within the same module, a comparison of the expression patterns between the two varieties revealed that both the blue

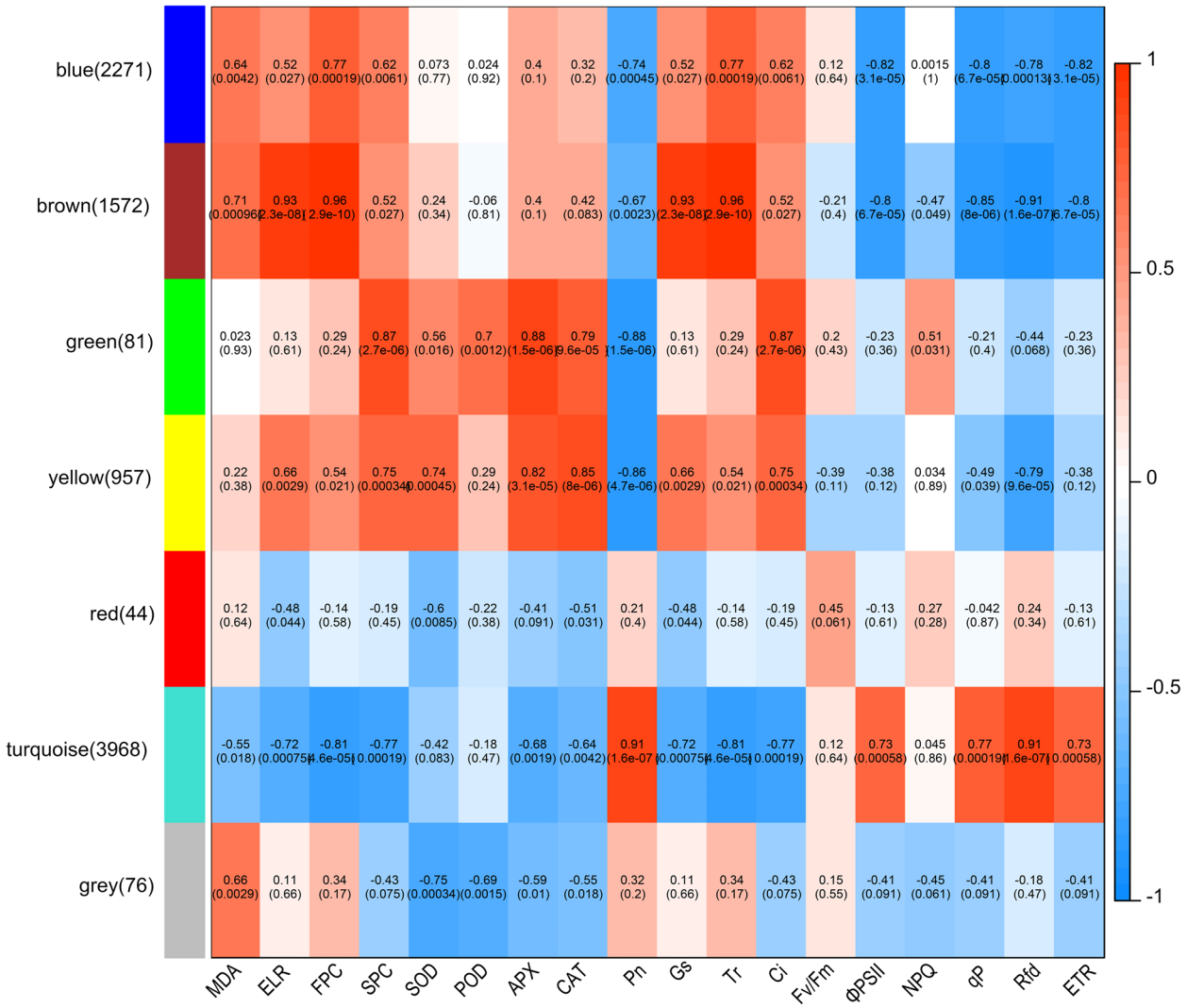

Fig. 5 Correlation analysis and corresponding P value between physiological traits and modules. MDA, MDA content; ELR, electrolyte leakage rate; FPC, free proline content; SPC, soluble protein content. SOD, SOD activity; CAT, CAT activity; APX, APX activity; CAT, CAT activity. Pn, net photosynthetic rate; Gs, stomatal conductance; Tr, transpiration rate; Ci, intercellular CO_2 concentration; Fv/Fm, maximum photosystem II (PSII) light quantum efficiency; ΦPSII, actual photochemical efficiency; NPQ, non-photochemical quenching coefficient; qP, photochemical quenching coefficient; Rfd, fluorescence decay rate; ETR, electron transfer rate

and brown modules exhibited an upward trend in gene expression following NaCl stress. However, this increase was significantly more pronounced in FH23. Additionally, there were notable differences in gene expression within the green and yellow modules, with a greater increase observed in NH5. The expression levels of genes in the blue-green module were found to be similar. Therefore, it is hypothesized that the genes in the blue, brown, green, and yellow modules are closely associated with salt tolerance in peanuts. These four modules are key contributors to the differences in salt tolerance observed between the two varieties.

Gene co-expression network construction and hub gene screening

In order to identify the key genes regulating physiological traits in the core module, the top 200 genes from each of the 4 key modules were selected for co-expression network analysis, and the six genes with the highest connectivity were taken as hub genes (Fig. 6). In the blue module, the hub genes encode delta-1-pyrroline-5-carboxylate synthase (P5CS, *LOC112748454*), phosphatidate phosphatase PAH1 (PAH, *LOC112705836*), 2-oxoglutarate-Fe(II) type oxidoreductase (*LOC112751263*), probable magnesium transporter NIPA1 (*LOC112792656*),

temperature-induced lipocalin-1 (TIL, *LOC112723412*), and cold-regulated 413 plasma membrane (*LOC112788918*). And these genes were more abundantly expressed in FH23 than in NH5. In the brown module, the hub genes encoded aldehyde dehydrogenase (ALDH, *LOC112710495*), Shewanella-like protein phosphatase 2 (*LOC112697303*), AAA-ATPase ASD, mitochondrial (*LOC112716352*), indole-3-pyruvate monooxygenase (*LOC112758300*), and functional positional proteins (*LOC112802216*, *LOC112795723*). In the green module, the hub genes encode nuclear transcription factor Y subunit A-1 (NFYA, *LOC112791664*), SNF1-related protein kinase (SnRK, *LOC112741331*), blue copper proteins (BCPs, *LOC112723292*), ethylene-responsive transcription factor 9 (ERF, *LOC112737698*), heavy metal-associated isoprenylated plant protein 9 (*LOC112765582*), and probable receptor-like protein kinase At5g24010 (RLKs, *LOC112744183*). In the yellow module, the hub genes encode chaperone proteins (ClpB1, *LOC112722577*, *LOC112709701*), 17.3 kDa class I heat shock protein (HSP, *LOC112733527*, *LOC112777158*), heat shock homologue 70 kDa protein (*LOC112736623*) and histone H1 (*LOC112792004*), genes from this module were significantly upregulated in NH5 (Table 1).

Discussion

Soil salinity has long been a significant constraint to crop growth and development globally, and therefore research on crop responses to salt stress has been of considerable interest [27]. As an important source of high-quality plant protein and vegetable oil, peanut is extremely tolerant to barrenness and is usually grown on marginal lands such as arid and saline soils [28]. Consequently, enhancing the selection and development of salt-tolerant peanut varieties has emerged as the most effective and economical strategy to increase yields and expand cultivated areas in salinized regions [29].

Excessive soil salinity in salinized soils induces salt stress in crops, leading to a significant accumulation of toxic ions such as Na^+ and Cl^- in the crop. This ionic imbalance disrupts the physiological processes of the crops, resulting in osmotic stress that ultimately affects their growth and development [30]. The cell membrane is the first component of the plant to be compromised when it encounters salt stress [31]. The sustained stress responses have been shown to cause considerable damage to cell membranes, impairing their integrity, fluidity, and selective permeability. This damage facilitates the leakage of large amounts of intracellular substances, ultimately resulting in the loss of cellular function [32]. Malondialdehyde (MDA) serves as an indicator of the extent of cell membrane damage, with MDA levels increasing when plants are subjected to stress [9]. Hussain et al. [33] demonstrated that MDA content rises under salt stress, regardless of the plant's tolerance level to such stress. Furthermore, the sensitive variety exhibited a more pronounced increase in MDA levels compared to the salt-tolerant varieties. These findings are consistent with those of the present study, which revealed that MDA content in peanut leaves significantly increased following NaCl stress, with a more substantial rise observed in FH23 compared to NH5. This suggests that FH23 may have experienced more severe oxidative damage. In this study, we found that the free proline and soluble protein contents of NH5 exhibited a consistent upward trend and remained elevated under continuous NaCl stress. Proline is a crucial osmoregulatory compound that plays a significant role in osmoregulation [34]. However, there is ongoing debate regarding the specific role of proline in this process. Proline acts as a protective agent, accumulating in salt-tolerant genotypes and facilitating effective osmoregulation, thereby enhancing salt tolerance [35, 36]. The results of our study indicated that the free proline content in peanut leaves increased following the imposition of salt stress. Notably, FH23 exhibited a higher free proline content. A similar conclusion was drawn from the study by Guo et al. [37], which found that sensitive varieties had higher proline content than salt-tolerant varieties. Conversely, another perspective suggests that proline is not directly involved in alleviating osmotic stress. It functions as a scavenger of reactive oxygen species and a stabilizer of membrane structure to help resist stress conditions [38]. The proline content in leaves and roots, as well as the salt tolerance of 132 different alfalfa varieties, were analyzed for correlations. The results indicated that proline exhibited distinct behaviors in roots compared to leaves. Additionally, root salt tolerance was positively correlated with overall salt tolerance, while leaf proline content showed a negative correlation with salt tolerance [39]. Concurrently, stress conditions were associated with alterations in the activities of antioxidant enzymes. Gurmani et al. found that SOD and POD activity were elevated in two pea varieties subjected to salt stress [40]. A similar pattern was observed in the present study, where the NH5 exhibited increased antioxidant enzyme activities compared to the sensitive peanut varieties. This enhancement may enable NH5 to better resist oxidative damage induced by salt stress through the elevated activities of SOD, POD, APX, and CAT (Fig. 7).

The production of photosynthetic products is a crucial factor influencing yield formation [41]. Leaves are the first part of the plant to be impacted by salt stress and serve as the most important organ for photosynthesis, which is often inhibited by both stomatal and non-stomatal limiting factors [19]. When plants are initially exposed to salt stress, the normally open stomata on their

Table 1 Description and expression of hub genes

Gene	Description	Expression (-2 log$_2$FC 9)					
		SS-0h	SS-24h	SS-48h	ST-0h	ST-24h	ST-48h
Blue							
LOC112748454	delta-1-pyrroline-5-carboxylate synthase	1.31	7.02	7.17	1.75	5.92	5.99
LOC112705836	phosphatidate phosphatase PAH1	3.41	5.61	5.56	3.12	4.76	4.72
LOC112751263	2-oxoglutarate-Fe(II) type oxidoreductase	3.84	6.03	5.72	3.88	5.2	5.01
LOC112792656	probable magnesium transporter NIPA1	4.99	7.45	6.41	5.29	6.51	5.94
LOC112723412	temperature-induced lipocalin-1	0.42	4.64	4.79	0.14	3.78	3.79
LOC112788918	cold-regulated 413 plasma membrane	4.29	7.47	7.56	4.57	6.67	6.71
Brown							
LOC112802216	uncharacterized protein LOC107490413	5.42	6.87	7.24	5.38	6.38	6.52
LOC112795723	uncharacterized protein LOC107482765	3.4	5.76	6.29	3.55	5.33	5.36
LOC112710495	probable aldehyde dehydrogenase	3.39	8.04	8.72	3.93	7.14	7.59
LOC112697303	shewanella-like protein phosphatase 2	1.11	2.81	3.56	0.91	2.6	2.66
LOC112716352	AAA-ATPase ASD, mitochondrial	-0.6	3.83	4.92	-0.6	2.99	3.21
LOC112758300	probable indole-3-pyruvate monooxygenase YUCCA10	3.49	6.06	6.58	3.6	5.36	5.63
Green							
LOC112791664	nuclear transcription factor Y subunit A-1	3.53	6.19	5.65	4.07	6	5.87
LOC112741331	SNF1-related protein kinase regulatory subunit beta-2	1.64	3.02	2.68	1.61	3.15	3.14
LOC112723292	blue copper protein	1.85	4.05	4.05	1.13	4.6	3.72
LOC112737698	ethylene-responsive transcription factor 9	2.79	5.19	5.84	3.33	6.07	5.59
LOC112765582	heavy metal-associated isoprenylated plant protein 9	-0.6	1.57	0.95	-0.8	1.59	1.23
LOC112744183	probable receptor-like protein kinase At5g24010	1.41	3.07	3.18	1.5	3.59	2.39
Yellow							
LOC112722577	chaperone protein ClpB1	0.54	4.55	6.2	0.33	5.75	6.92
LOC112709701	chaperone protein ClpB1	1.73	4.48	5.93	1.67	5.59	6.6
LOC112733527	17.3 kDa class I heat shock protein	4.34	6.58	8.18	4.02	8.12	9.05
LOC112777158	17.3 kDa class I heat shock protein	-0.9	5.3	6.93	-1.1	6.63	7.82
LOC112736623	heat shock cognate 70 kDa protein 2	3.67	6.46	7.92	3.74	7.78	8.51
LOC112792004	histone H1	5.79	5.02	6.67	5.51	6.76	7.56

leaves tend to close. This closure disrupts the exchange of CO_2, O_2, and other gases between plant cells, significantly impairing photosynthesis, a phenomenon referred to as stomatal limitation [42]. As salt stress persists, the damage to the plant intensifies, leading to limitations in cellular metabolism and the destruction of tissue structure. Metabolic disorders occur and stomatal factors are no longer the primary influences on plant photosynthesis. Instead, non-stomatal limiting factors have emerged as the main contributors to the decline in the photosynthetic rate [32]. In this study, the parameters Pn, Gs, Tr, and Ci significantly decreased at the onset stage (6 h) of NaCl stress, with stomatal limitations identified as the primary factor contributing to the reduction in the photosynthetic rate. Fv/Fm is a crucial indicator of photosynthetic efficiency in plants. It remains stable

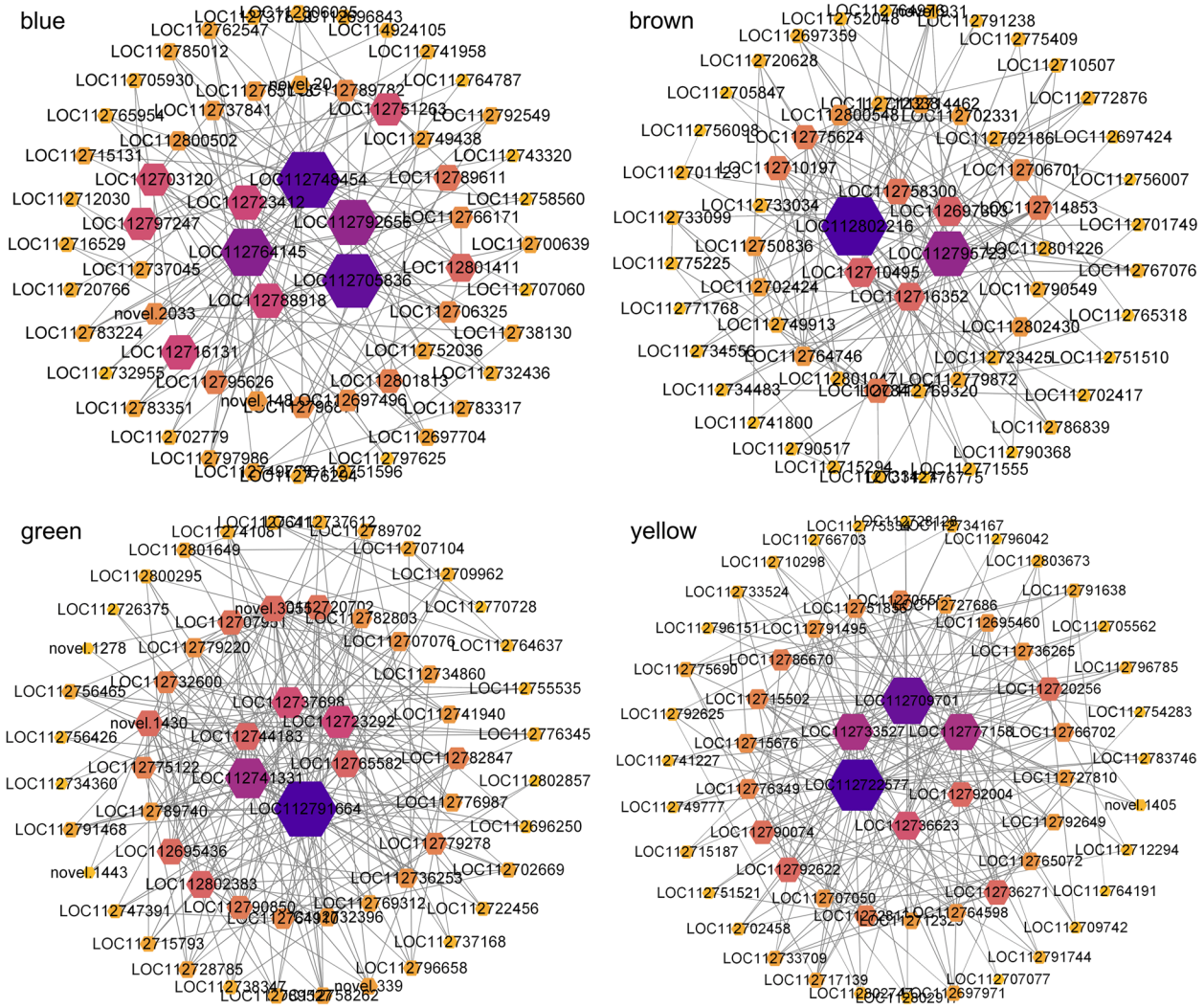

Fig. 6 Gene expression profiles of highly correlated co-expression modules

under healthy physiological conditions and only declines when the plant experiences stress-related damage [43]. Fv/Fm did not change significantly at 6 h. To avoid damage to photosynthetic organs, ΦPSII, qP, ETR, and Rfd also showed a decreasing trend; to mitigate the damage caused by excess light energy, NPQ increased significantly to dissipate the excess light energy in the form of heat energy [44]. ΦPSII, qP, and ETR gradually recovered, while NPQ also increased significantly during 6 h to 24 h of NaCl stress. This suggests that various regulatory mechanisms within the plant may have played a role in maintaining normal physiological activities during this period. Plant photosynthesis primarily depends on chlorophyll to capture light energy. However, prolonged salt stress can lead to chlorophyll degradation. In this study, chlorophyll a in NH5 began to decompose at 48 h whereas FH23 showed signs of decomposition as early as 12 h. Fv/Fm, ΦPSII, qP, ETR, and NPQ began to decline after 48 h of NaCl stress, with a significant decrease observed after 72 h. The decline in FH23 was even more pronounced. This indicates that as the duration of NaCl stress increases, the salt damage to the plants intensifies, leading to impairment of cellular metabolism and tissue structure. Consequently, this results in an imbalance of the regulatory mechanisms within the plants, preventing them from maintaining normal physiological functions. Conversely, the Ci of FH23 began to increase after 48 h of NaCl stress and was significantly higher after 72 h. The metabolism of FH23 cells was seriously affected, the photosynthetic rate decreased, CO_2 consumption decreased, resulting in an increase in interstitial CO_2 concentration, while the change of NH5 was not obvious. The electrolyte leakage rate and MDA content of the plant increased significantly after 48 h of salt stress, and the FH23 increased

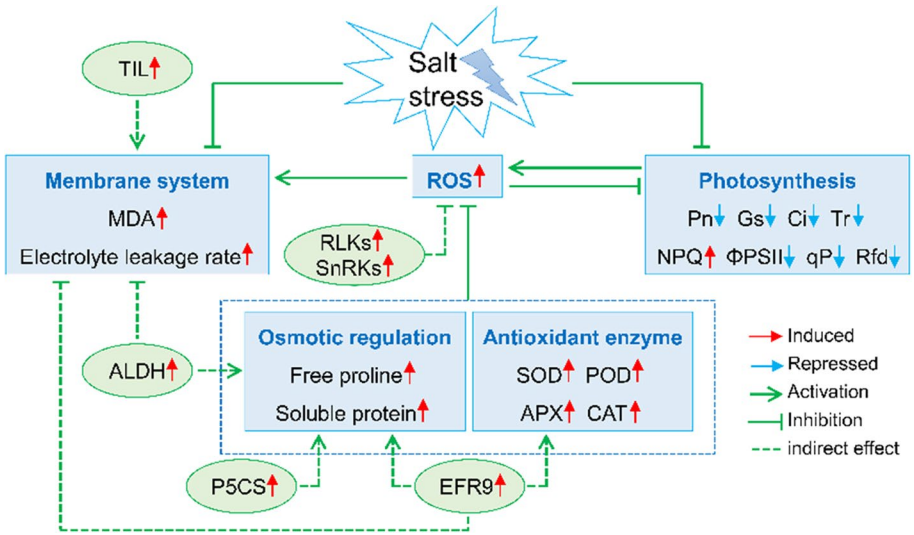

Fig. 7 Potential NaCl tolerance regulation mechanism in peanut revealed by WGCNA

more, indicating that the cell membrane structure was damaged and many contents were extravasated. In summary, stomatal limiting factors were the main reason for the decrease in photosynthetic rate at the beginning of the stress, and non-stomatal limiting factors were the main limiting factors with the extension of the stress time. The metabolism of FH23 cells was significantly affected, leading to a decrease in the photosynthetic rate and CO_2 consumption, which resulted in an increase in interstitial CO_2 concentration. In contrast, the changes observed in NH5 were not as pronounced. The electrolyte leakage rate and MDA content of the plants increased significantly with FH23 exhibiting a more substantial increase after 48 h of salt stress. This indicates that the cell membrane structure was compromised, resulting in the leakage of cellular contents. Chloroplasts as essential components of the cell membrane involved in photosynthesis were also impacted [45]. In summary, stomatal limitations were the primary reason for the initial decrease in the photosynthetic rate during the onset of stress, while non-stomatal factors became the predominant limiting factors as the duration of stress extended.

Through WGCNA, 4 key modules were identified. The gene expression patterns within the same module were similar; however, expression levels varied among different tolerant peanut varieties. It was hypothesized that these variations are key factors contributing to differences in varietal tolerance. Hub genes play a crucial role in specific physiological processes as the genes with the highest degree of connectivity to other genes in the co-expression network [14]. The *LOC112748454* gene identified in the blue module, encodes P5CS, a rate-limiting enzyme in proline synthesis. This enzyme catalyzes the conversion of glutamate-to-glutamate semialdehyde (GSA), which is subsequently auto-cyclized and converted to proline by pyrrolidine-5-carboxylic acid reductase (P5CR). The increase in proline content observed in the present study may be attributed to the up-regulation of the P5CS gene (Fig. 7), consistent with findings that demonstrate P5CS accumulation in chickpeas following salt stress, which leads to proline accumulation [46]. Furthermore, 3 hub genes encoding cell membrane proteins were identified. One of which, *LOC112723412* (TIL), exhibited a significant increase in expression after exposure to stress. TIL1 is localized in the plasma membrane and plays a crucial role in maintaining membrane stability under abiotic stress. Inhibition of TIL1 expression during salt stress suppresses the degradation of chlorophyll b and mitigates membrane damage [47]. Among the 4 hub genes identified in the brown module, the expression of *LOC112710495* (ALDH) significantly increased following NaCl stress. ALDH functions as an aldehyde scavenger, utilizing $NADP^+$ or NAD^+ to convert acetaldehyde into acetic acid, thereby reducing toxic compounds and producing NADPH or NADH in the process. This reduction in lipid peroxidation contributes to the regulation of abiotic stress [48]. Furthermore, the overexpression of the *ALDH21* gene enhances salt tolerance and drought resistance in both tobacco and cotton [49].

In the green module, *LOC112741331* (SnRK) and *LOC112744183* (RLKs) encode protein kinases that play crucial roles in multiple signaling pathways related to abiotic stress [50]. SnRK2 acts as a positive regulator of ABA signaling by phosphorylating downstream ABF [51], which subsequently helps protect against damage caused by abiotic stress [52]. In addition, SnRK2s can

directly regulate osmotic pressure independently of ABA, thereby promoting plant growth and development [30]. The expression of CeqSnRK3.16 was significantly upregulated under various salt stress conditions in Mucuna pruriens, indicating its potential as a candidate gene for salt stress tolerance [53]. In this study, *LOC112741331* (SnRK) was significantly upregulated under NaCl stress, particularly in the NH5, indicating that it may be a candidate gene for salt tolerance in peanuts. Additionally, *LOC112737698* (ERF9) exhibited a significant increase following NaCl stress, with a more pronounced elevation observed at 48 h. ERF9 is a member of the ERF family, which plays a crucial role in the response to abiotic stress (Fig. 7). One study found that the overexpression of the *LoERF017* gene could lead to increased activities of SOD and POD, as well as decreased levels of MDA and ROS in larch plants. This suggests that the overexpression of the *LoERF017* gene may enhance the osmotic resistance of plants by inducing antioxidant enzyme systems [54]. Potatoes that overexpress the StERF94 transcription factor exhibit resistance to oxidative stress damage by increasing antioxidant enzyme activity and the synthesis of osmoregulatory substances, which, in turn, improves salt tolerance [55]. In the yellow module, the hub gene comprises three genes encoding HSP proteins. The expression of HSP genes (*HSP 17.8*, *HSP 26.3*, *HSP 70*, and *HSP 101*) was found to be elevated under salt stress in wheat with a more pronounced increase observed in drought-tolerant wheat cultivars compared to drought-susceptible ones [56]. Similar findings have also been documented in grapevines where 14 genes encoding HSPs were significantly upregulated following salt stress [57]. In Arabidopsis thaliana, HsfA4a senses ROS accumulation and regulates the oxidative stress response under oxidative stress conditions [58]. The HSP genes (*LOC112733527*, *LOC112777158*, and *LOC112736623*) in peanuts showed a significant increase after NaCl stress, with the increase in NH5 being even more pronounced, suggesting that HSPs have a positive regulatory effect on salt stress (Fig. 7). Accordingly, a potential regulatory network for salt tolerance in peanuts was constructed in this study.

Conclusion

In this study, we analyzed the physiological and molecular responses of salt-tolerant and salt-sensitive peanut seedlings to NaCl stress by comparing physiological parameters and transcriptomic data. Under continuous NaCl stress, the electrolyte leakage rate in peanut leaves increased, indicating damage to membrane permeability, with FH23 experiencing more severe damage. NH5 maintains intracellular osmotic homeostasis by accumulating free proline and soluble protein content. Additionally, NH5 exhibits high antioxidant enzyme activity particularly in CAT and APX. At the onset of NaCl stress, photosynthetic parameters significantly decreased, with stomatal limitation identified as the primary restricting factor. Salt stress exacerbates damage to peanuts, adversely affecting cellular metabolism and tissue structure. This disruption leads to an imbalance in the regulatory mechanisms of peanuts, preventing them from maintaining normal physiological activities as stress duration increases. Subsequently, non-stomatal limiting factors became the main contributors to the decline in photosynthesis observed in FH23. We constructed a potential salt tolerance regulatory network in peanuts based on WGCNA, which identified 4 key co-expression modules and 24 hub genes regulating P5CS, TIL, ALDH, SnRKs, and HSP. The proposed mechanisms underlying these processes are illustrated in Fig. 7. Our comprehensive study elucidated the response mechanisms of peanut seedlings to NaCl stress and identified several candidate genes, providing a foundation for the selection of salt-tolerant peanut varieties.

Methods

Plant materials and stress treatment

The experiment was conducted in a hydroponic shed at the experimental base of Shenyang Agricultural University (41°50′ N, 123°34′ E). In this experiment, two peanut varieties, i.e., Nonghua5 (NH5, salt-tolerant, bred by Shenyang Agricultural University) and Fuhua23 (FH23, salt-sensitive, bred by Aeolian Sand Research Institute of Liaoning Academy of Agricultural Sciences), which were selected from 57 varieties in the previous study, were used as test materials [59]. Uniformly full seeds were selected and sterilized with sodium hypochlorite (NaOCl). They were then soaked in distilled water for 8 h to fully absorb, after which they were germinated by the paper bedding. Seeds exhibiting uniform germination were sown in vermiculite pots and irrigated with 1/2 Hoagland nutrient solution (PH0424, Phygene, Fuzhou, China). The cotyledons were removed after 14d and transplanted to a hydroponic tank with 1/2 Hoagland nutrient solution for 3d. Subsequently, supplemented with 200 mM NaCl to the 1/2 Hoagland nutrient solution. The hydroponic tanks were aerated with an air pump, and the nutrient solution was replaced with fresh nutrient solution every 3d. The nutrient solution lost due to evaporation was replenished with distilled water on a daily basis, additionally. The inverted trifoliate leaves of peanut seedlings were collected at 0 h, 6 h, 12 h, 24 h, 48 h, 72 h, and 96 h, respectively, wrapped in tin foil, and immediately frozen in liquid nitrogen. They were subsequently stored in a − 80 °C refrigerator.

Physiological measurement

Malondialdehyde (MDA) content was determined using the thiobarbituric acid (TBA) colorimetric method [60]. Each experiment was repeated three times. Take leaves 0.5 g and put them in 10 ml of trichloroacetic acid (TCA). After grinding and centrifuging, absorb 1.5 ml of supernatant and add 2.5 ml of 5% TCA containing 0.5% TBA. The mixture was evenly mixed, heated in boiling water bath for 15 min and then iced in water bath immediately. The supernatant was centrifugated at 8000r for 10 min at 4 °C. The absorption value of the supernatant was determined by spectrophotometer at 532 nm and 600 nm to calculate the MDA content.

And free proline content was determined using the acid ninhydrin colorimetric method [60]. Each experiment was repeated three times. Take leaves 0.5 g and add 10 ml 3% sulfosalicylic acid solution in a glass tube, and bathe in boiling water for 10 min. After cooling, take 2 ml supernatant add 2 ml glacial acetic acid and 4 ml acid ninhydrin reagent, and develop color in boiling water bath for 1 h. After cooling 5 ml toluene was added, the red substance was extracted by full shock. The toluene layer was taken after static layering and then the light absorption value was determined by spectrophotometer at 520 nm.

Electrolyte leakage rate was measured using a conductivity meter (DDSJ-308F, Shanghai, China) [61]. Each experiment was repeated three times. The leaves were rinsed with deionized water. The round pieces of leaves were taken by a punch (diameter, 8 mm). Take 20 round pieces of leaves in tube with 20 ml deionized water. The electrolyte leakage rate (E0) was measured immediately after shaking. The electrolyte leakage rate E1 was measured at room temperature for 4 h. Heated in boiling water bath for 30 min, the electrolyte leakage rate after cooling is E2. Electrolyte leakage rate = (E1-E0)/(E2-E0) × 100%.

The soluble protein content was determined by using Coomassie Brilliant Blue G250 staining [62]. Each experiment was repeated three times. Take leaves 0.5 g, cut them and put into a pre-cooled mortar, add 5 ml distilled water and grind thoroughly. The extraction solution was poured into 10 ml tube and centrifugated at 3000r for 10 min at 4 °C. Absorb 1.0 ml of supernatant into a clean tube and add 5 ml of Coomassie Brilliant Blue G250. After the mixture was uniformly placed for 2 min, the absorption value was measured at 595 nm by spectrophotometer.

The crude antioxidant enzyme solution was extracted from 0.5 g of leaves using sodium phosphate buffer. Superoxide dismutase (SOD) activity was assessed using the photochemical Nitro Blue Tetrazolium (NBT) method, while peroxidase (POD) activity was determined using the guaiacol method [63]. Add 1.5 ml of 50 mM sodium phosphate buffer (pH = 7.8), 0.3 ml of 75 μM NBT solution, 0.3 ml of 10 μM Na_2-EDTA, 0.25 ml of distilled water, 0.3 ml of 20 μM riboflavin, 0.3 ml of 130 mM methionine (Met) solution and 50 μl of crude enzyme solution successively into 10 ml clear beaker. The samples were then placed in a dark environment to terminate the reaction after 20 min of reaction. The SOD activity was calculated by measuring the light absorption value at 560 nm with microplate reader. 50 μl of crude enzyme solution was reacted with 0.95 ml of 0.2% guaiacol, 1 ml of 0.3% H_2O_2 and 1 ml of 50 mM sodium phosphate buffer (pH = 5.5), the absorption value at 470 nm was determined, and POD activity was calculated. Each experiment was repeated three times.

Catalase (CAT) activity was determined using hydrogen peroxide decomposition reaction method [64]. Each experiment was repeated three times. The reaction solution was prepared by adding 154.6 μl of 30% H_2O_2 to a beaker containing 100 ml of 0.1 M sodium phosphate buffer (pH = 7.0) mixing well and storing at 37 °C. 0.1 ml of crude enzyme solution was taken and reacted with 2.9 ml of reaction solution in a water bath at 37 °C and the absorption value at 240 nm was determined. 1.8 ml of 0.1 M sodium phosphate buffer (pH = 7.0), 0.1 ml of 15 mM ascorbic acid solution, 1 ml of 0.3 mM H_2O_2, and 0.1 ml crude enzyme solution were added into the clean enzyme label plate successively. The absorption value of 290 nm was determined and the APX activity was calculated.

Photosynthetic parameters and chlorophyll fluorescence parameters

The leaf photosynthetic parameters were determined using a CIRAS-2 portable photosynthetic (Hansatech, UK). The conditions within the leaf chamber were as follows: temperature 25 °C, relative humidity 70%, light intensity 1200 μmol m^{-2} s^{-1}, and CO_2 concentration 380 μmol m^{-2} s^{-1}. 15 plants (5 plants per replicate) were randomly selected for each treatment with uniform growth. The net photosynthetic rate (Pn), stomatal conductance (Gs), transpiration rate (Tr) and intercellular CO_2 concentration (Ci) of fully expanded inverted trifoliate leaves of peanut were measured at 0 h, 6 h, 24 h, 48 h, 72 h and 96 h of NaCl stress. Leaf chlorophyll fluorescence parameters were determined with a FluorCam FC800 chlorophyll imaging system (Photon Systems Instruments, Czech Republic). 15 plants (5 plants per replication) exhibiting uniform growth were randomly selected for each treatment. The fully expanded inverted trifoliate leaves of the peanuts were harvested at 0 h, 6 h, 12 h, 24 h, 48 h, 72 h, and 96 h of NaCl stress. The leaves were then wrapped in moistened gauze and covered with tinfoil to maintain a certain level of humidity and to

prevent curling and wilting. Following 30 min dark treatment to avoid light exposure, the maximum photosystem II (PSII) light quantum efficiency (Fv/Fm), non-photochemical quenching coefficient (NPQ), actual photochemical efficiency (ΦPSII), photochemical quenching coefficient (qP), electron transfer rate (ETR), and fluorescence decay rate (Rfd) were determined.

Transcriptome sequencing

Transcriptome analysis of peanut leaves was conducted at 0 h, 24 h, and 48 h with three replicates for each treatment. RNA was extracted using the Plant RNA Extraction Kit (Tiangen, China). The purity, concentration, and integrity of the RNA were assessed. After the samples passed quality control, mRNA with a poly-A tail was enriched using Oligo-dT magnetic beads. The enriched mRNA was then randomly fragmented, and the resulting fragments served as templates for synthesizing the first strand of cDNA. This cDNA was subsequently degraded to synthesize the second strand, which was then purified. The purified double-stranded cDNA underwent end-repair, A-tailing, and ligation to sequencing adapters, followed by screening with AMPure XP beads (Beckman Coulter, Pasadena, CA). PCR amplification was performed on the cDNA, and the PCR products were purified again using AMPure XP beads to obtain the final library. 0.4 μg of treated total RNA was used as the template for each reverse transcription reaction. Once library construction was completed, preliminary quantification was performed using Qubit 2.0 (Thermo, Waltham, MA, USA). Fluorometer, followed by assessment of the insert size using an Agilent 2100 Bioanalyzer, which met the expected criteria. qRT-PCR was employed to accurately determine the effective concentration of the library, ensuring its quality. Clean data were obtained by filtering the downstream data using fastp v0.19.3. Sequencing was carried out on the Illumina NovaSeq 6000 system. The clean reads were compared with the cultivated peanut genome (arah.tifrunr.gnm1.kyv3). FPKM values were calculated based on the comparison, and *p*-values were corrected using the Benjamini and Hochberg method. The corrected *p*-value and the absolute value of Log_2FC were used as thresholds for expressing significant differences. $|log_2FC| \geq 1.0$ with $FER < 0.05$ was used as the differential gene screening condition [26].

Weighted gene co-expression network analysis

Gene co-expression networks were constructed with validly expressed ($FPKM \geq 1$) genes through the software WGCNA v1.71 package in R Studio. Following the scale-free principle, the power value (soft threshold) was determined by the pickSoftThreashold function. The gene co-expression network was visualized by Cytoscape software and hub genes were identified in each module.

Quantitative real-time PCR analysis (qRT-PCR)

Total RNA was extracted using the Plant RNA Extraction Kit (Tiangen, China). qRT-PCR was performed using the SYBR Premix Ex Taq Kit (TaKaRa, China). The cycling parameters were as follows: an initial denaturation at 95 °C for 10 min, followed by 40 cycles of denaturation at 95 °C for 15 s and annealing at 60 °C for 30 s. Each sample was analyzed in triplicate. The relative gene expression was calculated using the $2^{-\Delta\Delta CT}$ method [65]. The gene primers for qRT-PCR are listed in Table S1.

Statistical analysis

Statistical analyses of data were performed using Microsoft Excel 2016 (Microsoft Corporation, USA) and SPSS 22 (SPSS Inc., USA). Graphs were drawn using GraphPad Prism 8.0.2 (GraphPad Software Inc., USA), R 3.4.4 software. Data between different time points for the same species were analyzed using one-way analysis of variance (ANOVA). A value of $p < 0.05$ was deemed to be statistically significant.

Supplementary Information

The online version contains supplementary material available at https://doi.org/10.1186/s12870-025-06311-5.

Additional file 1: Fig. S1 Morphological characteristics of NH5 and FH23 under NaCl stress.

Additional file 2: Fig. S2 qRT-PCR verification of peanut transcriptome date under NaCl stress.

Additional file 3: Fig. S3 WGCNA of effectively expressed genes in NH5 and FH23 under NaCl. (A) Filtering of WGCNA network power values. (B) Hierarchical clustering trees of gene co-expression networks. (C) Correlation heat maps of gene co-expression networks.

Additional file 4: Fig. S4. Gene expression profiles of highly correlated co-expression modules.

Additional file 5: Table S1. The primers used in qRT-PCR.

Additional file 6: Table S2. Statistics of transcriptome sequencing and reference genome alignment of peanut leaf samples under control and salinity stress.

Clinical trial number

Not applicable.

Authors' contributions

HY and NZ conceived and designed the experiments. NZ, BB and SZ performed all the lab experiments. NZ, HZ, and JR conducted the field trials and collected the samples for RNASeq. NZ, ZL and DZ performed WGCNA and data processing. NZ drafted the manuscript. HY, HZ and NZ revised the manuscript. All authors have read and agreed to the published version of the manuscript.

Funding
This work was supported by the earmarked fund for "Yingkou Talent Plan" science and technology leading talents project, CARS-13.

Data availability
The RNA-Seq data have been submitted to the NCBI Sequence Read Archive (SRA; http://www.ncbi.nlm.nih.gov/sra/, accessed on 18 November 2023) database with the accession number PRJNA1041034.

Declarations

Ethics approval and consent to participate
Not applicable.

Consent for publication
Not applicable.

Competing interests
The authors declare no competing interests.

Author details
[1]College of Agronomy, Shenyang Agricultural University, Shenyang 110161, China. [2]School of Agriculture and Horticulture, Liaoning Agricultural Vocational and Technical College, Yingkou 115009, China.

Received: 11 October 2024 Accepted: 26 February 2025
Published online: 06 March 2025

References

1. Han M, Cui R, Wang D, Huang H, Rui C, Malik WA, et al. Combined transcriptomic and metabolomic analyses elucidate key salt-responsive biomarkers to regulate salt tolerance in cotton. BMC Plant Biol. 2023;23(1):245–62.
2. Abbas G, Rehman S, Siddiqui MH, Ali HM, Farooq MA, Chen Y. Potassium and humic acid synergistically increase salt tolerance and nutrient uptake in contrasting wheat genotypes through ionic homeostasis and activation of antioxidant enzymes. Plants (Basel, Switzerland). 2022;11(3):263–80.
3. Liang S, Wang S, Zhou L, Sun S, Zhang J, Zhuang L. Combination of biochar and functional bacteria drives the ecological improvement of saline-alkali soil. Plants (Basel, Switzerland). 2023;12(2):284–96.
4. Bonku R, Yu J. Health aspects of peanuts as an outcome of its chemical composition. Food Sci Human Wellness. 2020;9(1):21–30.
5. Patel J, Khandwal D, Choudhary B, Ardeshana D, Jha RK, Tanna B, et al. Differential physio-biochemical and metabolic responses of peanut (Arachis hypogaea L.) under multiple abiotic stress conditions. Int J Mol Sci. 2022;23(2):660–82.
6. Munns R. Comparative physiology of salt and water stress. Plant, Cell Environ. 2002;25(2):239–50.
7. Chrysargyris A, Papakyriakou E, Petropoulos SA, Tzortzakis N. The combined and single effect of salinity and copper stress on growth and quality of *Mentha spicata* plants. J Hazard Mater. 2019;368:584–93.
8. Ganapati RK, Naveed SA, Zafar S, Wang W, Xu J. Saline-Alkali Tolerance in Rice: Physiological Response, Molecular Mechanism, and QTL Identification and Application to Breeding. Rice Sci. 2022;29(5):412–34.
9. Wang H, Li Z, Ren H, Zhang C, Xiao D, Li Y, et al. Regulatory interaction of BcWRKY33A and BcHSFA4A promotes salt tolerance in non-heading Chinese cabbage [Brassica campestris (syn. Brassica rapa) ssp. chinensis]. Horticulture Res. 2022;9:113–30.
10. Panda SK, Khan MH. Growth, oxidative damage and antioxidant responses in greengram (Vigna radiata L.) under short-term salinity stress and its recovery. J Agronomy Crop Sci. 2009;195(6):442–54.
11. Li W, Feng Z, Zhang C. Ammonium transporter PsAMT1.2 from Populus simonii functions in nitrogen uptake and salt resistance. Tree Physiol. 2021;41(12):2392–408.
12. Hua J, Wua X, Wua F, Chena W, Whiteb JC, Yangc Y, et al. Potential application of titanium dioxide nanoparticles to improve the nutritional quality of coriander (Coriandrum sativum L.). J Hazard Mater. 2020;389:121837–47.
13. Yao C, Li X, Li Y, Yang G, Liu W, Shao B, et al. Overexpression of a *Malus baccata* MYB transcription factor gene *MbMYB4* increases cold and drought tolerance in *Arabidopsis thaliana*. Int J Mol Sci. 2022;23(3):1794–811.
14. Ren J, Guo P, Zhang H, Shi X, Ai X, Wang J, et al. Comparative physiological and coexpression network analyses reveal the potential drought tolerance mechanism of peanut. BMC Plant Biol. 2022;22(1):460–75.
15. Li S, Yu J, Li Y, Zhang H, Bao X, Bian J, et al. Heat-responsive proteomics of a heat-sensitive spinach variety. Int J Mol Sci. 2019;20(16):3872–92.
16. Zhang JJ, Jo JO, Huynh DL, Mongre RK, Ghosh M, Singh AK, et al. Growth-inducing effects of argon plasma on soybean sprouts via the regulation of demethylation levels of energy metabolism-related genes. Sci Rep. 2017;7:41917–28.
17. Qian J, Lu B, Chen H, Wang P, Wang C, Li K, et al. Phytotoxicity and oxidative stress of perfluorooctanesulfonate to two riparian plants: *Acorus calamus* and *Phragmites communis*. Ecotoxicol Environ Saf. 2019;180:215–26.
18. Yan K, He W, Bian L, Zhang Z, Tang X, An M, et al. Salt adaptability in a halophytic soybean (*Glycine soja*) involves photosystems coordination. BMC Plant Biol. 2020;20(1):155–67.
19. Jańczak-Pieniążek M, Migut D, Piechowiak T, Balawejder M. Assessment of the impact of the application of a quercetin-copper complex on the course of physiological and biochemical processes in wheat plants (Triticum aestivum L.) growing under saline conditions. Cells. 2022;11(7):1141–56.
20. Sahoo RK, Tuteja R, Gill R, Bremont JFJ, Gill SS, Tuteja N. Marker-free rice (Oryza sativa L. cv. IR 64) overexpressing PDH45 gene confers salinity tolerance by maintaining photosynthesis and antioxidant machinery. Antioxidants (Basel, Switzerland). 2022;11(4):770–81.
21. Zeeshan M, Lu M, Naz S, Sehar S, Cao F, Wu F. Resemblance and Difference of Seedling Metabolic and Transporter Gene Expression in High Tolerance Wheat and Barley Cultivars in Response to Salinity Stress. Plants (Basel, Switzerland). 2020;9(4):519–35.
22. Chinnusamy V, Jagendorf A, Zhu JK. Understanding and Improving Salt Tolerance in Plants. Crop Sci. 2005;45(2):437–48.
23. Quan R, Wang J, Hui J, Bai H, Lyu X, Zhu Y, et al. Improvement of Salt Tolerance Using Wild Rice Genes. Front Plant Sci. 2018;8:2269–79.
24. Qian G, Wang M, Wang X, Liu K, Li Y, Bu Y, et al. Integrated Transcriptome and Metabolome Analysis of Rice Leaves Response to High Saline-Alkali Stress. Int J Mol Sci. 2023;24(4):4062–82.
25. Zhang Y, Gao X, Li J, Gong X, Yang P, Gao J, et al. Comparative analysis of proso millet (Panicum miliaceum L.) leaf transcriptomes for insight into drought tolerance mechanisms. BMC Plant Biol. 2019;19(1):397–413.
26. Zhang N, Zhang H, Lv Z, Bai B, Ren J, Shi X, et al. Integrative multi-omics analysis reveals the crucial biological pathways involved in the adaptive response to NaCl stress in peanut seedlings. Physiol Plant. 2024;176(2):14266–79.
27. Zhou Z, Wang J, Yu Q, Lan H. Promoter activity and transcriptome analyses decipher functions of CgbHLH001 gene (Chenopodium glaucum L.) in response to abiotic stress. BMC Plant Biol. 2023;23(1):116–39.
28. Zhu H, Jiang Y, Guo Y, Huang J, Zhou M, Tang Y, et al. A novel salt inducible WRKY transcription factor gene, *AhWRKY75*, confers salt tolerance in transgenic peanut. Plant Physiol Biochem. 2021;160:175–83.
29. Xu T, Meng S, Zhu X, Di J, Zhu Y, Yang X, et al. Integrated GWAS and transcriptomic analysis reveal the candidate salt-responding genes regulating Na+/K+ balance in barley (Hordeum vulgare L.). Front Plant Sci. 2022;13:1004477–97.
30. Liaqat A, Alfatih A, Jan SU, Sun L, Zhao P, Xiang C. Transcription elongation factor AtSPT4-2 positively modulates salt tolerance in *Arabidopsis thaliana*. BMC Plant Biol. 2023;23(1):49–61.
31. Sun M, Liu X, Gao H, Zhang B, Peng F, Xiao Y. Phosphatidylcholine Enhances Homeostasis in Peach Seedling Cell Membrane and Increases Its Salt Stress Tolerance by Phosphatidic Acid. Int J Mol Sci. 2022;23(5):2585–601.
32. Ji X, Tang J, Fan W, Li B, Bai Y, He J, et al. Phenotypic differences and physiological responses of salt resistance of walnut with four rootstock types. Plants (Basel, Switzerland). 2022;11(12):1557–76.
33. Hussain S, Bai Z, Huang J, Cao X, Zhu L, Zhu C, et al. 1-methylcyclopropene modulates physiological, biochemical, and antioxidant responses of rice to different salt stress levels. Front Plant Sci. 2019;10:124–41.

34. Chen J, Liu Y, Zhang T, Zhou Z, Huang J, Zhou T, et al. Integrated physiological and transcriptional dissection reveals the core genes involving nutrient transport and osmoregulatory substance biosynthesis in allohexaploid wheat seedlings under salt stress. BMC Plant Biol. 2022;22(1):502–20.
35. Chen F, Fang P, Peng Y, Zeng W, Zhao X, Ding Y, et al. Comparative proteomics of salt-tolerant and salt-sensitive maize inbred lines to reveal the molecular mechanism of salt tolerance. Int J Mol Sci. 2019;20(19):4725–46.
36. Mulaudzi T, Hendricks K, Mabiya T, Muthevhuli M, Ajayi RF, Mayedwa N, et al. Calcium improves germination and growth of sorghum bicolor seedlings under salt stress. Plants. 2020;9(6):730–47.
37. Guo X, Ahmad N, Zhao S, Zhao C, Zhong W, Wang X, et al. Effect of salt stress on growth and physiological properties of asparagus seedlings. Plants (Basel, Switzerland). 2022;11(21):2836–49.
38. Kim J, Liu Y, Zhang X, Zhao B, Childs KL. Analysis of salt-induced physiological and proline changes in 46 switchgrass (*Panicum virgatum*) lines indicates multiple response modes. Plant Physiol Biochem. 2016;105:203–12.
39. Kang Y, Torres-Jerez I, An Z, Greve V, Huhman D, Krom N, et al. Genome-wide association analysis of salinity responsive traits in *Medicago truncatula*. Plant, Cell Environ. 2019;42(5):1513–31.
40. Gurmani AR, Wang X, Rafique M, Jawad M, Khan AR, Khan QU, et al. Exogenous application of gibberellic acid and silicon to promote salinity tolerance in pea (Pisum sativum L.) through Na+ exclusion. Saudi J Biol Sci. 2022;29(6):103305–13.
41. Bharali A, Baruah KK. Effects of integrated nutrient management on sucrose phosphate synthase enzyme activity and grain quality traits in rice. Physiol Mol Biol Plants. 2022;28(2):383–9.
42. Singh R, Parihar P, Singh S, Mishra RK, Singh VP, Prasad SM. Reactive oxygen species signaling and stomatal movement: Current updates and future perspectives. Redox Biol. 2017;11:213–8.
43. Lu X, Ma L, Zhang C, Yan H, Bao J, Gong M, et al. Grapevine (*Vitis vinifera*) responses to salt stress and alkali stress: transcriptional and metabolic profiling. BMC Plant Biol. 2022;22(1):528–49.
44. Ma M, Liu Y, Bai C, Yang Y, Zhang S, Han X, et al. The physiological functionality of PGR5/PGRL1-dependent cyclic electron transport in sustaining photosynthesis. Front Plant Sci. 2021;12:702196–702194.
45. Li C, Ran M, Liu J, Wang X, Wu Q, Zhang Q, et al. Functional analysis of CqPORB in the regulation of chlorophyll biosynthesis in *Chenopodium quinoa*. Front Plant Sci. 2022;13:1083438–51.
46. Kaur G, Sanwal SK, Sehrawat N, Kumar A, Kumar N, Mannb A. Getting to the roots of Cicer arietinum L. (chickpea) to study the effect of salinity on morpho-physiological, biochemical and molecular traits. Saudi J Biol Sci. 2022;29(12):103464–76.
47. Abo-Ogiala A, Carsjens C, Diekmann H, Fayyaz P, Herrfurth C, Feussner I, et al. Temperature-induced lipocalin (TIL) is translocated under salt stress and protects chloroplasts from ion toxicity. J Plant Physiol. 2014;171(3–4):250–9.
48. Zhao J, Missihoun TD, Bartels D. The role of Arabidopsis aldehyde dehydrogenase genes in response to high temperature and stress combinations. D - 9882906. 2017;68(15):4295–4308.
49. Yang H, Zhang D, Zhang D, Bozorov TA, Abdullaev AA, Wood AJ, et al. Overexpression of *ALDH21* from syntrichia caninervis moss in upland cotton enhances fiber quality, boll component traits, and physiological parameters during deficit irrigation. Crop Sci. 2019;59:553–64.
50. Chen X, Ding Y, Yang Y, Song C, Wang B, Yang S, et al. Protein kinases in plant responses to drought, salt, and cold stress. J Integr Plant Biol. 2021;63(1):53–78.
51. Katsuta S, Masuda G, Bak H, Shinozawa A, Kamiyama Y, Umezawa T, et al. Arabidopsis Raf-like kinases act as positive regulators of subclass III SnRK2 in osmostress signaling. Plant J. 2020;103(2):634–44.
52. Nishimura N, Tsuchiya W, Moresco JJ, Hayashi Y, Satoh K, Kaiwa N, et al. Control of seed dormancy and germination by DOG1-AHG1 PP2C phosphatase complex via binding to heme. Nat Commun. 2018;9(1):2132–44.
53. Ai D, Wang Y, Wei Y, Zhang J, Meng J, Zhang Y. Comprehensive identification and expression analyses of the *SnRK* gene family in *Casuarina equisetifolia* in response to salt stress. BMC Plant Biol. 2022;22(1):572–89.
54. Hu X, Xu X, Li C. Ectopic expression of the *LoERF017* transcription factor from *Larix olgensis* Henry enhances salt and osmotic-stress tolerance in *Arabidopsis thaliana*. Plant Biotechnology Reports. 2018;12(2):93–104.
55. Charfeddine M, Charfeddine S, Ghazala I, Bouaziz D, Bouzid RG. Investigation of the response to salinity of transgenic potato plants overexpressing the transcription factor StERF94. J Biosci. 2019;44(6):141–56.
56. Khateeb WA, Muhaidat R, Alahmed S, Zoubi MSA, Al-Batayneh KM, El-Oqlah A, et al. Heat shock proteins gene expression and physiological responses in durum wheat (*Triticum durum*) under salt stress. Physiol Mol Biol Plants. 2020;26(8):1599–608.
57. Zhao F, Zheng T, Liu Z, Fu W, Fang J. Transcriptomic analysis elaborates the resistance mechanism of grapevine rootstocks against salt stress. Plants (Basel, Switzerland). 2022;11(9):1167–83.
58. Yang Y, Guo Y. Unraveling salt stress signaling in plants. J Integr Plant Biol. 2018;60(9):796–804.
59. Zhang N, Zhang H, Ren J, Bai B, Guo P, Lv Z, et al. Characterization and comprehensive evaluation of phenotypic and yield traits in salt-stress-tolerant peanut germplasm for conservation and breeding. Horticulturae. 2024;10(2):147–64.
60. Heath RL, Packer L. Photoperoxidation in isolated chloroplasts: I. Kinetics and stoichiometry of fatty acid peroxidation. Arch Biochem Biophys. 1968;125(1):189–98.
61. Zhao DY, Shen L, Fan B, Liu KL, Yu MM, Zheng Y, et al. Physiological and genetic properties of tomato fruits from 2 cultivars differing in chilling tolerance at cold storage. J Food Sci Technol. 2009;74(5):C348-352.
62. Sedmak JJ, Grossberg SE. A rapid, sensitive, and versatile assay for protein using Coomassie brilliant blue G250. Anal Biochem. 1977;79(1–2):544–52.
63. Ling F, Su Q, Jiang H, Cui J, He X, Wu Z, et al. Effects of strigolactone on photosynthetic and physiological characteristics in salt-stressed rice seedlings. Sci Rep. 2020;10(1):6183–90.
64. Wei Z, Gao T, Liang B, Zhao Q, Ma F, Li C. Effects of exogenous melatonin on methyl viologen-mediated oxidative stress in apple leaf. Int J Mol Sci. 2018;19(1):316–29.
65. Livak KJ, Schmittgen TD. Analysis of relative gene expression data using real-time quantitative PCR and the $2^{-\Delta\Delta CT}$ method. Methods. 2001;25(4):402–8.

Publisher's Note